2015 American Control Conference
Palmer House Hilton
July 1-3, 2015. Chicago, IL, USA

Control-Oriented MIMO Modeling of Laser-Aided Powder Deposition Processes*

Xiaoqing Cao and Beshah Ayalew

Abstract— **This paper proposes a control-oriented multiple input multiple output (MIMO) model for a class of laser aided powder deposition (LAPD) processes. First, the various components of a multi-physics model of LAPD processes are briefly reviewed including the laser-powder interaction, heat transfer with phase change, fluid flow and surface deformation. The difficulty of capturing these nonlinear, coupled, spatio-temporal multi-physical interactions via lumped parameter modeling is highlighted. Then, a new MIMO model is derived in Hammerstein form by concatenating a linearized dynamics with coupled nonlinear relationships derived from mass and heat balance considerations. This MIMO model captures the coupled dynamics with laser power and scanning speed as inputs and deposited layer height and melting pool temperature as outputs. To identify the unknown model parameters, a constrained optimization problem is solved using the detailed multi-physics models. The MIMO model is in a form suitable for multivariable control designs for LAPD processes.**

Keywords: laser-aided powder deposition, control-oriented MIMO model, additive manufacturing

I. INTRODUCTION

Laser-aided powder deposition (LAPD) encompasses a wide range of modern additive manufacturing processes such as laser cladding, selective laser sintering (SLS), laser metal deposition (LMD) and laser solid freeform fabrication (LSFF) [1, 2]. In LAPD processes, a high-intensity laser beam is employed as a heat source that sweeps across the surface of the substrate, creating a melting pool. The powder material is either preplaced on the substrate or injected into the melting pool by coaxial or lateral powder nozzles. After melting and solidification processes, a metallurgical bond is formed between the deposited layer and the substrate. Metallic parts can then be manufactured in a layer by layer manner. Compared with conventional material processing techniques, LAPD processes are reported to have advantages in energy and material utilization efficiency and process productivity [1, 3].

A persistent challenge with LAPD processes is achieving high dimensional accuracy, surface finish and overall product quality. Model-based control system designs could help in this regard. However, the prevailing spatio-temporal multi-physical phenomena, namely, heat transfer with phase change on the substrate, thermo-capillary induced fluid flow in the melting pool, free surface deformation as well as the laser-powder interaction are closely described by nonlinear partial differential equations (PDEs). While such PDE-based models offer accurate and explicit representations of these physical interactions, their high computational burden limits their use even for efficient open-loop simulations. Although some model simplifications have been achieved by reduction techniques such as the enhanced thermal conductivity method [4], the computational cost associated with PDE-based models prohibits their use for practical, online implementable control system designs.

By comparison, lumped parameter models are often preferred candidates in process control for their ability to succinctly capture particular input-output relations. These are often ordinary differential equation (ODE) based descriptions extracted from input-output data, relating individual inputs (laser power, scanning speed or powder mass flow) to specific outputs (melting pool temperature or deposited layer height/width). In [5], a fourth-order linear state-space model was identified to represent the transient response of melting pool temperature with respect to laser power in a laser cladding process. In [6], Hofman et al. proposed an Autoregressive Exogenous (ARX) model to represent the dynamic relation between laser power and melting pool width. Similarly in [7], a second order transfer function was obtained from recorded data to describe the relation between laser power and melting pool temperature. Considering mass balance, a knowledge-based Hammerstein model was proposed in [8] for a LSFF process, where only the relationship between the laser scanning speed and the layer height was characterized. However, as pointed out in [5], LAPD is a complicated process where the multiple inputs of laser power, scanning speed and powder feedrate need to be simultaneously manipulated for regulating or tracking multiple process outputs such as the deposited layer height and melting pool temperature. Therefore, MIMO control system designs are a requirement for LAPD processes in order to achieve acceptable product quality. This evokes the need for suitable models that can capture the inherent coupled interactions of LAPD processes while retaining the potential use of the models for online implementable control system designs.

In this paper, a control-oriented MIMO process model is proposed for LAPD processes. This model describes the coupled nonlinear dynamics of deposited layer height and melting pool temperature with laser power and scanning speed as process input variables. We construct the MIMO model in Hammerstein form [9], where static nonlinear relationships are first derived from explicit mass and heat balance considerations for the melting pool, and then connected to first-order linear dynamics blocks. The unknown parameters

*Research supported, in part, by U.S. National Science Foundation under Grant No. CMMI-1055254, and the U.S. Department of Energy (DOE) GATE Program under Grant No. DE-EE0005571

Xiaoqing Cao and Beshah Ayalew are with the Applied Dynamics and Control Group at the Clemson University-International Center for Automotive Research, Greenville, SC 29607 USA (e-mail: {xiaoqin, beshah@clemson.edu}).

for the MIMO model are obtained by using parameter identification experiments on finite element simulations of the complete multi-physics model. The proposed model aims to fill the identified gap in suitable models for MIMO control system design of LAPD processes.

The rest of the paper is organized as follows: Section II presents a detailed discussion on the multi-physics modeling of LAPD processes. Section III presents the assumptions adopted in this paper and details the derivation of the proposed MIMO process model. Section IV provides the identification of unknown parameters in the proposed model. Conclusions about the proposed model and further applications of this model are included in Section V.

II. Multi-physics Model of LAPD Processes

Due to their explicit considerations of the aforementioned physical phenomena, PDE-based models are often considered to be more accurate since inherent spatio-temporal distributions of the process state are preserved. The following is a brief discussion of the main models for the sub-processes in a coaxial nozzle and laser set up shown in Fig. 1:

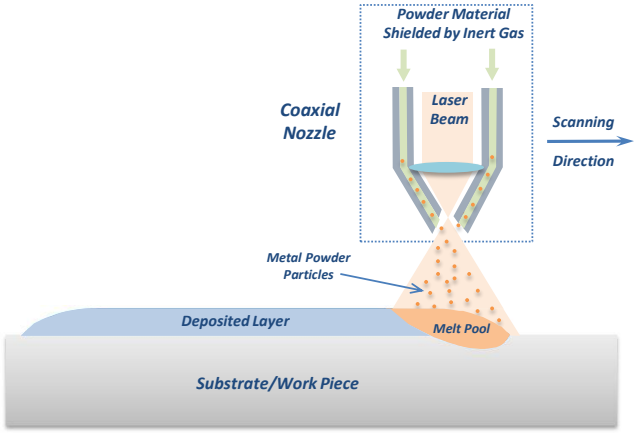

Fig. 1. Schematic of the LAPD processes

1. Laser-Powder Interaction

The laser irradiation intensity under the coaxial nozzle head can be expressed by [10]:

$$I(x,z) = \frac{2q}{\pi w^2} * e^{-\frac{2(x-x_0)^2}{w^2}} \tag{1}$$

where q is the total power contained in the laser beam; $w = w_0\left(1+\frac{\varsigma^2}{z_R{}^2}\right)^{1/2}$ is the Gaussian beam radius and $\varsigma = \varsigma(z)$ is particle traveling distance from the nozzle exit; w_0 and z_R are initial Gaussian beam radius and Raleigh range, respectively. x_0 denotes the position of the laser source.

During the time from powder injection at the nozzle to powder deposition into the melting pool, the powder particles and the laser beam interact with each other, leading to the attenuation of the laser irradiation power even before it is absorbed by the substrate and creates the melting pool. This attenuation effect of laser power can be approximated via Beer-Lambert's law:

$$I_{att}(x,z) = I(x,z) * e^{-A*\alpha_{ext}*n*\varsigma} \tag{2}$$

where A denotes the mean particle cross sectional area, α_{ext} is the extinction coefficient. n is the number of particles per unit volume and can be formulated as [11]:

$$n(x,z) = \frac{3\dot{m}_P}{2v_P\rho_P\pi^2\sigma_P^2 r_P^3} * e^{\frac{-2(x-x_0)^2}{\sigma_P^2}} \tag{3}$$

where $\dot{m}_P$ is the powder feedrate, v_P, r_P and ρ_P represent the average flying velocity, particle radius and density, respectively. σ_P is the powder distribution parameter that denotes the stream radius reaching $1/e^2$ of the maximum powder concentration. Then, the attenuated laser power distribution on the substrate surface is given by:

$$I_{att}(x) = \alpha_{att}(x) * q \tag{4}$$

with the power attenuation coefficient α_{att} expressed by:

$$\alpha_{att}(x) = \frac{2}{\pi w^2} e^{-\frac{2(x-x_0)^2}{w^2} - \frac{3\alpha_{ext}\dot{m}_P z_0}{2\pi v_P\rho_P r_p\sigma_P^2} * e^{\frac{-2(x-x_0)^2}{\sigma_P^2}}} \tag{5}$$

where z_0 is the distance from the coaxial nozzle head to the substrate and is assumed to be constant for the process.

2. Heat Transfer with Phase Change (HTPC)

In LAPD processes, the melting pool created by the high intensity laser source involves heat transfer with phase change, resulting in a binary solid-liquid (S/L) phase system. The HTPC problems are challenging to model because the latent heat transfer within the mushy zone (where solid and liquid coexist) during the melting process has to be taken into account. One way to include this is to use a mixture model where local material properties in the computational domain are modeled via temperature-dependent functions. The modified material heat capacity, which is also known as the apparent heat capacity, can be described as follows [12]:

$$C_p = (1-\alpha_l)C_{ps} + \alpha_l C_{pl} + \mathcal{L}\frac{d\alpha_l}{dT} \tag{6}$$

where C_p is the heat capacity with s and l denoting the values for the solid and liquid phase, separately. $\mathcal{L}$ is the latent heat of fusion and is assumed to be a material-dependent constant. α_l is a smooth temperature-dependent function that represents the local volumetric fraction of the liquid phase. Similarly, the density ρ and heat conductivity k of this S/L binary system can be approximated by:

$$\begin{cases} \rho = \dfrac{(1-\alpha_l)\rho_s C_{ps} + \alpha_l\rho_l C_{pl}}{(1-\alpha_l)C_{ps} + \alpha_l C_{ps}} \\ k = (1-\alpha_l)k_s + \alpha_l k_l \end{cases} \tag{7}$$

Note that although these material properties are modeled with these uniform expressions for the solid, liquid and mushy zones, they depend on the local temperature as implied by the distributed parameter α_l. Then, the HTPC model can be derived based on energy balance as follows:

$$\rho C_p\frac{\partial T}{\partial t} + \rho C_p u\cdot\nabla T = \nabla\cdot(k\nabla T) \tag{8}$$

where u is fluid velocity. The boundary conditions can be expressed as:

$$\begin{cases} k\dfrac{\partial T}{\partial \boldsymbol{n}} = \alpha_{att} * q + h(T - T_\infty) + \varepsilon\sigma(T^4 - T_\infty^4),\ \Gamma_{top} \\ k\dfrac{\partial T}{\partial \boldsymbol{n}} = h(T - T_\infty) + \varepsilon\sigma(T^4 - T_\infty^4), \Gamma/\Gamma_{top} \end{cases} \quad (9)$$

where $\boldsymbol{n}$ is the outward vector normal to the surface. The top surface (Γ_{top}) of the substrate is subjected to attenuated laser irradiation as well as natural convection and radiation with the ambient. For other surfaces (Γ/Γ_{top}), only convective and radiative heat transfer are assumed. The initial temperature of the substrate may be taken as ambient temperature T_∞.

3. Fluid Flow and Surface Deformation

With the high-intensity laser irradiation, high temperature gradients often occur at the top surface of the melting pool, leading to a non-uniform surface tension which drives liquid particles to move from low to high surface tension regions. This is often referred as 'Marangoni-driven flow'. Although the Marangoni effect has been identified as dominant in melting pools [13], other forces such as the gravity force and buoyancy force also exist. The fluid flow driven by the combination of all these forces affects the geometry of the melting pool. The fluid flow in the melting pool is modeled by the well-known Navier-Stokes equation:

$$\begin{cases} \rho\dfrac{\partial u}{\partial t} + \rho(u \cdot \nabla)u = \nabla \cdot [-pI + \mu(\nabla u + (\nabla u)^T)] + F \\ \rho\nabla \cdot u = 0 \end{cases} \quad (10)$$

where F denotes the combined forces. To include the Marangoni effect, a boundary condition which represents the balance between the thermo-capillary force and the viscous force can be established as [14]:

$$\mu\frac{\partial u}{\partial n} = \frac{d\gamma}{dT}\frac{\partial T}{\partial s} \quad (11)$$

where γ is the temperature-dependent surface tension and s denotes the tangential direction. No-slip boundary conditions are assumed for the other boundaries of the substrate.

To overcome the computational difficulties associated with the multi-physics coupling, particularly of the fluid flow effects, the enhanced thermal conductivity method has been previously proposed for similar applications. The basic idea is to enhance the thermal conductivity in the melting pool to represent the effect of fluid flow induced by the Maragoni effect. This method was experimentally validated in [4]. In this paper, we shall similarly adopt an enhanced thermal conductivity for the melting pool as follows:

$$k_l^* = \alpha_{ETC} * k_l \quad (12)$$

where α_{ETC} is the enhancing factor applied in the liquid domain.

As the powder material is injected and deposited into the melting pool, the surface geometry of the melting pool deforms and later solidifies into a new deposited layer. This deformation can be modeled in terms of the motion of the melting surface in the normal direction. Considering the mass balance of the powder material, the layer increment rate can be modeled as:

$$V_n = \frac{N_p\eta\dot{m}_P}{\pi\rho_P{\sigma_P}^2}e^{-N_p\left(\frac{x-x_0}{\sigma_P}\right)^2} \quad (13)$$

where η is the powder catch efficiency and N_p is the constriction coefficient [15]. This melting pool surface deformation can be implemented as the normal mesh velocity via the Arbitrary Lagrange-Euler (ALE) method.

4. Finite Element Simulations

The above sub-models of the multi-physics phenomena involved in LAPD processes were implemented in the finite element software COMSOL for simulating deposition on a low-carbon steel substrate of dimension $20mm \times 3m$ with over 14000 triangular mesh elements. Inconel 718 is used as the powder material for layer deposition [16]. The relevant parameters used for simulation are listed in Table I. With these simulation parameters and mesh type, the COMSOL finite element simulation took a computation time of 35939 s on a modern personal laptop (with 2.8 GHz CPU and 16GB RAM).

TABLE I. FINITE-ELEMENT SIMULATION PARAMETERS

Variable	Value	Variable	Value
q	600 $[W]$	$\rho_s(\rho_l)$	7870 $[kg/m^3]$
v	8 $[mm/s]$	C_{ps}/C_{pl}	658/ 804 $[J/kg/K]$
w_0	0.65 $[mm]$	k_s/k_l	40.9/43.9 $[W/m/K]$
z_R	1.25 $[m]$	$\mathcal{L}$	$2.71 * 10^5$ $[J/kg]$
r_P	50 $[\mu m]$	T_m	1809 $[K]$
v_P	5 $[m/s]$	T_∞	293 $[K]$
ρ_P	7784 $[kg/m^3]$	α_{ETC}	$diag[2,1]$
σ_P	3 $[mm]$	h	$10[W/m^2/K]$
$\dot{m}_P$	8 $[g/min]$	N_p	5
η	0.7		

The simulation result of the temperature distribution at $t = 0.6\ s$ is shown in Fig. 2 as an illustrative example. A new layer with the thickness around 0.3 mm is deposited at the rear side of the melting pool. The temperature distribution is asymmetric in the melting pool with respect to the position of the laser beam. By varying the control input variables, namely the laser power and scanning speed, measurable process outputs such as the deposited layer height and average melting pool temperature can be obtained and used for further analysis.

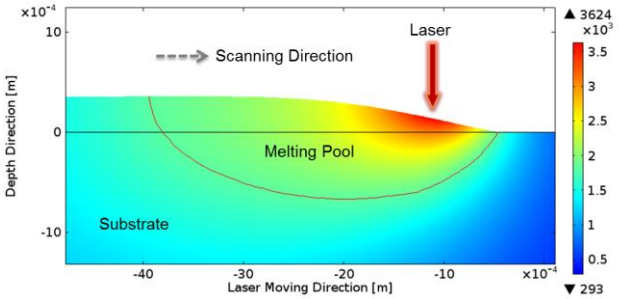

Fig. 2. Melting pool temperature at $t = 0.6\ s$

III. CONTROL-ORIENTED MIMO MODEL OF LAPD PROCESSES

As pointed out above, for efficient control system design and implementation, lumped parameter models that can

capture critical process dynamics while maintaining computational efficiency are desired. In order to derive such a control-oriented MIMO model for LAPD processes, we make the following simplifying assumptions: 1) The melting pool can be approximated by a semi-ellipse with length L, width W and height H as illustrated in the Fig. 3 [17]. 2) The melting pool aspect ratio (width/length) is empirically related to laser power q and scanning speed v via constants D, E as: $\frac{L}{W} = 1 + (Dq + E)v$ [18]. 3) The deposited track-width approximately remains constant and is determined by the laser beam diameter [19]. This constant track-width is denoted by W_0 in the rest of this paper.

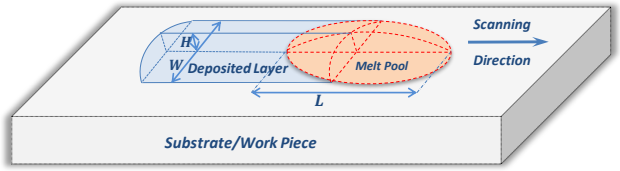

Fig. 3. Melting pool geometry

The derivation of the MIMO lumped model is based on the mass and energy balance equations suggested in [17], with modifications for temperature dependent powder catch efficiency and input dependent laser absorptivity. The mass balance in the melting pool can be expressed as:

$$\rho_l \dot{V} = \eta_m \dot{m}_P - \rho_l A v \tag{14}$$

where $V = \frac{\pi}{6} W_0 H L$ is the total volume of the melting pool; $A = \frac{\pi}{4} W_0 H$ is the cross-sectional area in the transverse plane; $\eta_m \dot{m}_P$ denotes the amount of powder material that is deposited into the melting pool in unit time and η_m is the powder catch efficiency (ratio of deposited powder to total injected powder), which is modeled as a function of melting pool temperature:

$$\eta_m(T) = \begin{cases} \eta_{m0} * \left[1 - e^{-k_T(T - T_m)}\right], T > T_m \\ 0, T \le T_m \end{cases} \tag{15}$$

where η_{m0} is the maximum powder catch efficiency and is assumed as a constant. The temperature dependence of the powder catch efficiency stems from the fact that the powder material is only deposited in the melting pool area (where $T > T_m$). The parameters of the function in (15) are affected by the nozzle configuration (laser beam distribution, powder distribution, etc.). For constant laser power and scanning speed, the melting pool moves at the same speed as the laser source and the pool geometry stays approximately the same in steady state. Thus, the steady-state deposited layer height can be derived by equating the left term in the mass balance equation to zero:

$$H_{ss} = \frac{4\eta_m \dot{m}_P}{\pi \rho_l W_0 v} \tag{16}$$

The heat transfer in the melting pool mainly consists of laser power absorption and heat convection between the solid-liquid and liquid-gas interfaces. The energy balance in the melting pool can be modeled as:

$$\rho_l(\dot{V}e) = \eta_q q - A_s h_s (T - T_m) - A_g h_g (T - T_0) - \delta_{S/L} \tag{17}$$

where e is the specific internal energy and is defined as: $e(T) = C_s(T_m - T_0) + \mathcal{L} + C_l(T - T_m)$. C_s and C_l denote the solid and liquid heat capacity, respectively, while $\mathcal{L}$ is the latent heat of fusion. $\eta_q q$ is the absorbed laser power in the melting pool and η_q denotes the laser absorptivity. Both the laser power and scanning speed affect the shape of the melting pool, which further determines the area of laser beam absorption. Therefore, laser absorptivity can be modeled as a function of laser power and scanning speed as follows:

$$\eta_q(q, v) = \eta_{q0} * (1 - e^{-k_q q}) * e^{-k_v v} \tag{18}$$

where η_{q0}, k_q, k_v are positive constants. The next two terms in the right side of (17) are heat convection on the liquid/solid and liquid/gas interfaces, respectively, where h_s and h_g are the respective heat convection coefficients. The heat convection area on these two interfaces can be expressed by $A_g = 2\pi * \left(\frac{\left(\frac{W_0}{2} * \frac{L}{2}\right)^{1.6} + \left(\frac{W_0}{2} * H\right)^{1.6} + \left(\frac{L}{2} * H\right)^{1.6}}{3} \right)^{\frac{1}{1.6}}$, $A_s = \frac{\pi}{4} W_0 L$. The last term $\delta_{S/L}$ in the energy balance equation represents the power outflow from the melting pool due to the effect of solidification and melting. In steady state, the melting pool moves at the same speed as the laser source and the surface geometry remains approximately the same. Therefore, the solidification and melting speed can be assumed the same and the term $\delta_{S/L}$ vanishes. Thus, the steady-state temperature can be derived as:

$$T_{ss} = \frac{\eta_q q + A_s h_s T_m + A_g h_g T_0}{A_s h_s + A_g h_g} \tag{19}$$

As pointed out in [8], LAPD processes are dominated by the thermal effects whose dynamics can be approximated with a first-order linear system. We concatenate this linear block with the expressions derived above that capture the nonlinear coupling in steady state. This is formally a Hammerstein type model as shown in the following figure:

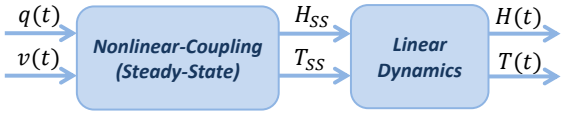

Fig. 4. Structure of the control-oriented process model

In this MIMO model, both the coupled dynamics of deposited layer height and melting pool temperature are approximated with a memoryless nonlinear function (steady-state relation) followed by a linear first-order block. The system dynamics equations are:

$$\begin{cases} \dot{H} = \frac{1}{\tau_H} * \left(\frac{4\eta_m \dot{m}_P}{\pi \rho_l W_0 v} - H \right) \\ \dot{T} = \frac{1}{\tau_T} * \left(\frac{\eta_q q + A_s h_s T_m + A_g h_g T_0}{A_s h_s + A_g h_g} - T \right) \end{cases} \tag{20}$$

where τ_H and τ_T are time constants. This model can be rewritten compactly as $Sys(H, T, U) = 0$, where $U = [q, v]^T$ is the input vector. In this proposed MIMO model, laser power and scanning speed are selected to be the control input variables. The powder feedrate is not considered as a control variable here. In practice, the response of the powder delivery system itself is so slow that it is better to pre-set it at constant

settings [7]. The two outputs are deposited layer height and melting pool temperature. Both of these two outputs are measureable via properly implemented sensors such as high-speed CCD cameras for deposited layer height sensing and radiation pyrometers for melting pool temperature measurement. It is important to note the two-way nonlinear coupling between the layer height and melting pool temperature is implied in the powder catch efficiency and heat convection areas included in the model. Moreover, the two control input variables are also nonlinearly involved in this model. These facts of the proposed model provide the possibility to capture the main characteristics of the complex interactions in LAPD processes. Furthermore, the dynamic model in (20) is in nonlinear state-space form, which enables the possibility of using it directly for advanced control system designs for LAPD processes. One such design is pursued in our companion paper [20]. Note also that while this MIMO model is suitable for LAPD processes with moving laser source, special attention should be paid to the singularity with $v = 0$ by providing a minimum operating speed. In the fully stationary case, where the scanning speed is identically zero, the system degrades to SIMO, and the above model does not apply.

IV. Parameter Identification

In this section, parameter identification is conducted on unknown parameters in the MIMO lumped model proposed in previous section. The parameters to be identified include: time constants τ_H, τ_T; empirical constants D, E in melting pool aspect ratio; powder catch efficiency parameters η_{m0}, k_T and laser absorptivity parameters η_{q0}, k_q and k_v. We use $X = [\tau_H, \tau_T, D, E, \eta_{m0}, k_T, \eta_{q0}, k_q, k_v]^T$ to denote the unknown parameter vector for brevity.

To obtain a set of plant data for parameter identification, the multi-physics process model introduced in section II is used as the plant because of its explicit considerations of the multi-physics phenomena and their interactions in the process. By predefining a control input sequence with variable laser power and scanning speed, the plant output data, namely the deposited layer height and average melting pool temperature are obtained from simulations in finite element software. Then, the parameter identification task is formulated as a constrained optimization problem as follows:

$$Min_X J(H, T, U) \tag{21}$$

$$Subject\ to: \quad Sys(H, T, U) = 0$$

The objective function $J(H, T, U)$ is defined as:

$$J = \int_t \left[\alpha_1 \left(\frac{H(\tau) - H_p}{\Delta H^*_{max}} \right)^2 + \alpha_2 \left(\frac{T(\tau) - T_p}{\Delta T^*_{max}} \right)^2 \right] d\tau \tag{22}$$

where ΔH^*_{max} and ΔT^*_{max} are the normalization constants correspond to the maximum expected deviations in layer height and melting pool temperature. α_1 and α_2 are positive weighting constants and they are assigned to be the same for equal optimization priority. Subscript p denotes the variables from the plant. This optimization is implemented in Matlab where the solution is obtained by the classical Nelder-Mead simplex method. The identified unknown parameters are listed in the following table.

TABLE II. IDENTIFIED PARAMETERS

Variable	Value	Variable	Value
τ_H	0.1145 $[s]$	η_{q0}	0.0545 [1]
τ_T	0.2898 $[s]$	k_q	$1.357 * 10^{-4}$ $[1/W]$
η_{m0}	0.4224 [1]	k_v	332.8 $[s/m]$
k_T	0.0072 [1/K]	D	-0.0769 $[s/m/W]$
		E	-0.9071 $[s/m]$

The control input sequences and the comparison results of the parameter identification experiments are illustrated in Figs. 5-7 as follows:

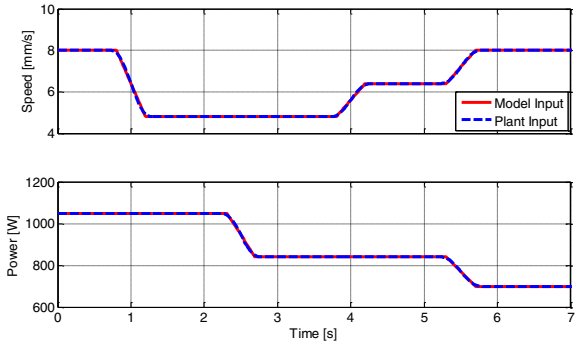

Fig. 5. Plant/model laser power and scanning speed

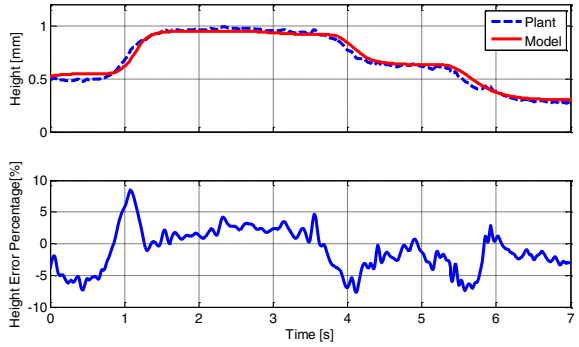

Fig. 6. Plant/model layer height comparison

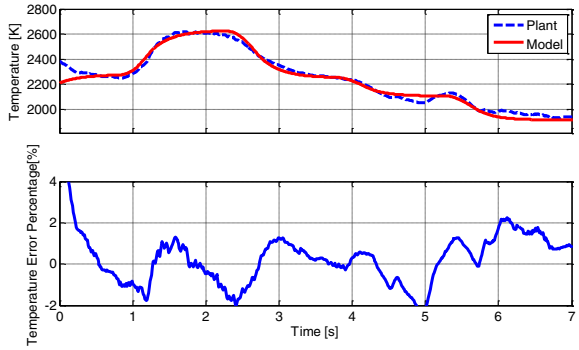

Fig. 7. Plant/model melting pool temperature comparison

Fig. 5 shows the input sequences, i. e., the combination of laser power and scanning speed used for parameter identification. They are assumed to be time-dependent step functions with sufficient smoothness for the finite element solver. The model/plant comparison of deposited layer height is shown in Fig. 6. We can see that the layer height from the proposed model follows the actual value in the plant fairly

well over the whole time range. The relative error (the root-mean-square-error with respect to the maximum values) of the layer height is 3.44%, which shows a relatively good agreement between the plant and the proposed model. Similarly, the comparison of average melting pool temperature is demonstrated in Fig. 7. It can be seen that the temperature output from the model shows some deviation from the actual plant value at the beginning. This is possibly due to the complex phase change dynamics occurring with the initial development of the melting pool, which is not considered in the proposed lumped model. Despite this, the proposed MIMO model captures the actual temperature dynamics well, with only a 1.32% relative error.

To further validate the proposed MIMO model with the identified parameters shown in Table II, a case study with different input sequences is also conducted and the plant/model comparison is illustrated in Fig.8.

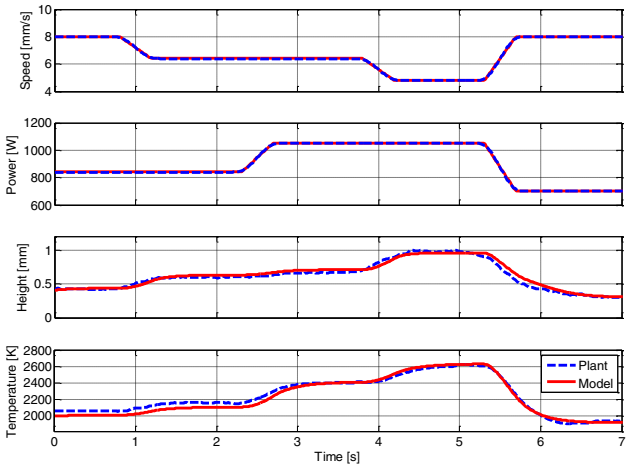

Fig. 8. Model validation

As we can see from the above figure, with the proposed model and identified parameters, the model outputs follow the plant outputs fairly closely. The relative errors are only 3.82% and 1.53% for layer height and pool temperature, respectively.

V. Conclusions

This paper proposed a control-oriented MIMO model for laser-aided powder deposition processes. Discussions of the multi-physical processes and corresponding models are offered. Then, by applying mass and energy balance in the melting pool, steady-state relations between multiple process inputs (laser power and scanning speed) and process outputs (deposited layer height and average melting pool temperature) are first established. By approximating the remaining dynamics as unknown first order system, a MIMO coupled nonlinear process model is obtained in Hammerstein form. The parameters of the proposed MIMO model are then properly calibrated through comparisons with results from a detailed multi-physics based process model. Having obtained a control-oriented MIMO model, it remains to explore multivariable control system designs for LAPD processes that utilize this model. In the companion paper submitted to this conference, a stable multivariable predictive control scheme is designed based on this model to simultaneously regulate or track the layer height and melting pool temperature in LAPD processes [20].

References

[1] J. Laeng, J. Stewart, and F. W. Liou, "Laser metal forming processes for rapid prototyping-A review," *International Journal of Production Research,* vol. 38, pp. 3973-3996, 2000.

[2] I. Gibson, D. W. Rosen, and B. Stucker, *Additive manufacturing technologies*: Springer, 2010.

[3] J. D. Majumdar and I. Manna, "Laser material processing," *International materials reviews,* vol. 56, pp. 341-388, 2011.

[4] A. Kamara, W. Wang, S. Marimuthu, and L. Li, "Modelling of the melt pool geometry in the laser deposition of nickel alloys using the anisotropic enhanced thermal conductivity approach," *Proceedings of the Institution of Mechanical Engineers, Part B: Journal of Engineering Manufacture,* vol. 225, pp. 87-99, 2011.

[5] L. Song and J. Mazumder, "Feedback control of melt pool temperature during laser cladding process," *Control Systems Technology, IEEE Transactions on,* vol. 19, pp. 1349-1356, 2011.

[6] J. Hofman, B. Pathiraj, J. van Dijk, D. de Lange, and J. Meijer, "A camera based feedback control strategy for the laser cladding process," *Journal of Materials Processing Technology,* 2012.

[7] D. Salehi and M. Brandt, "Melt pool temperature control using LabVIEW in Nd: YAG laser blown powder cladding process," *The international journal of advanced manufacturing technology,* vol. 29, pp. 273-278, 2006.

[8] A. Fathi, A. Khajepour, E. Toyserkani, and M. Durali, "Clad height control in laser solid freeform fabrication using a feedforward PID controller," *The International Journal of Advanced Manufacturing Technology,* vol. 35, pp. 280-292, 2007.

[9] K. Narendra and P. Gallman, "An iterative method for the identification of nonlinear systems using a Hammerstein model," *Automatic Control, IEEE Transactions on,* vol. 11, pp. 546-550, 1966.

[10] H. Qi, J. Mazumder, and H. Ki, "Numerical simulation of heat transfer and fluid flow in coaxial laser cladding process for direct metal deposition," *Journal of applied physics,* vol. 100, 024903, 2006.

[11] J. Liu, L. Li, Y. Zhang, and X. Xie, "Attenuation of laser power of a focused Gaussian beam during interaction between a laser and powder in coaxial laser cladding," *Journal of Physics D: Applied Physics,* vol. 38, p. 1546, 2005.

[12] A. Faghri and Y. Zhang, *Transport phenomena in multiphase systems*: Academic Press, 2006.

[13] R. Choo and J. Szekely, "Vaporization kinetics and surface temperature in a mutually coupled spot gas tungsten arc weld and weld pool," *Welding Journal(USA),* vol. 71, p. 77, 1992.

[14] Z. S. Saldi, "Marangoni driven free surface flows in liquid weld pools," *Ph.D. thesis, Delft University of Technology, Delft, Netherlands.,* 2012.

[15] S. Morville, M. Carin, P. Peyre, M. Gharbi, D. Carron, P. Le Masson, and R. Fabbro, "2D longitudinal modeling of heat transfer and fluid flow during multilayered direct laser metal deposition process," *Journal of Laser Applications,* vol. 24, p. 032008, 2012.

[16] A. J. Pinkerton, "An analytical model of beam attenuation and powder heating during coaxial laser direct metal deposition," *Journal of Physics D: Applied Physics,* vol. 40, p. 7323, 2007.

[17] C. Doumanidis and Y.-M. Kwak, "Geometry modeling and control by infrared and laser sensing in thermal manufacturing with material deposition," *Journal of manufacturing science and engineering,* vol. 123, pp. 45-52, 2001.

[18] A. J. Pinkerton and L. Li, "Modelling the geometry of a moving laser melt pool and deposition track via energy and mass balances," *Journal of Physics D: Applied Physics,* vol. 37, p. 1885, 2004.

[19] A. Fathi, E. Toyserkani, A. Khajepour, and M. Durali, "Prediction of melt pool depth and dilution in laser powder deposition," *Journal of Physics D: Applied Physics,* vol. 39, p. 2613, 2006.

[20] X. Cao and B. Ayalew, "Multivariable Predictive Control of Laser-Aided Powder Deposition Processes," in *American Control Conference (ACC)*, Chicago, IL, 2015.